Crystal Structure, Hirshfeld Surfaces and Energy Framework Studies of a Biologically Active Compound (3*E*)-3- (2,4- dimethoxybenzyldene) -2,3-dihydro- 4H-chromen-4-one

J. Hemalatha[1], D. Reuben Jonathan[2], D. Angeline Shirmila[1], M. Krishna Priya[1], K. Laavanya[3] and G. Usha[1*]

[1]*PG and Research Department of Physics, Queen Mary's College (A), Chennai-4. Affiliated to the University of Madras, Chennai-600004, Tamil Nadu, India.*
[2]*Department of Chemistry, Madras Christian college (A), Chennai-59. Affiliated to the University of Madras, Chennai-600004, Tamil Nadu, India.*
[3]*Department of Physics, DG Vaishnav college (A), Chennai-106, Affiliated to the University of Madras, Chennai-600004, Tamil Nadu, India.*

Authors' contributions

This work was carried out in collaboration among all authors. All authors read and approved the final manuscript.

Original Research Article

ABSTRACT

A new chalcone derivative (3*E*)-3-(2,4-dimethoxybenzyldene)-2,3-dihydro-4H-chromen-4-one (DBDB) has been synthesized by following the Claisen-Schmidt condensation reaction method at ambient temperature using the slow evaporation technique. The 3D crystal structure was solved using the single-crystal X-ray diffraction method (XRD). XRD intensity data reveal that the title compound crystallizes in an orthorhombic crystal system with non-centrosymmetric space group P2$_1$ 2$_1$ 2$_1$. The crystallographic parameters such as bond lengths, bond angles, torsion angles were estimated and are found to be in the normal range and comparable with the literature values. The

_____

Corresponding author: E-mail: guqmc@yahoo.com;

unit cell packing of the molecules shows that the adjacent molecules are linked via C-H…O hydrogen bonds. Hirshfeld surfaces namely d_{norm}, electrostatic potential, shape index, and curvedness were analyzed to visualize and to evaluate the weak intermolecular interactions, positive and negative potential regions, C-H…π, and π…π stacking interactions, respectively. The 2D fingerprint plots for the whole and delineated interactions were generated and analyzed to estimate their contributions to the total Hirshfeld surfaces. The pairwise intermolecular interactions were calculated as the sum of four scaled energy components namely electrostatic (E_{ele}), polarization (E_{pol}), dispersion (E_{dis}), and exchange-repulsion (E_{rep}) and graphically represented as energy frameworks. The energy frameworks analysis reveals that the total stabilizing energy is highly influenced by dispersion (E_{dis}) energy than the other components. In-vitro and in-silico investigations have also been performed for the title molecule which discloses the efficacious for use as a drug in inhibiting breast cancer cells without affecting the normal cells.

Keywords: Claisen-Schmidt condensation reaction; Hirshfeld surfaces; 2D fingerprint plots; Biological activity; In-vitro investigation; Cytotoxicity; Molecular docking; Anti-cancer activity evaluation.

1. INTRODUCTION

Cancer is a disease in which some of the body's cells grow uncontrollably and spread to other parts of the body. This fast-growing disease is anticipated to affect 22 million people by 2030 [1]. Fundamental Research at the molecular level on cancer attributes increases in the risk of getting cancer to low intake of fiber diet, small consumption of fruit and green vegetables, high consumption of red meats, alcohol consumption, smoking, higher intake of salt and saturated fats, etc. [2]. Also, increased exposure to UV radiation either occupational or general is one of the primary factors of cancer development. There are more than 100 types of cancer, which are usually named for the organs or tissues where the cancers form and specified by the type of cell that formed them, such as an epithelial cell or a squamous cell [3,4-5]. Breast cancer (BC) is a recurring and fatal ailment noticed in females. Its repercussions on the human population are enormous including the major cause of cancer deaths. Next to skin cancer, breast cancer is the most common cancer diagnosed, accounting for 23% of the total cancer cases and 14% of the cancer deaths [6-10,11]. Actually, BC does not symbolize a single disease but rather a number of molecularly distinct tumors arising from the epithelial cells of the breast [12-13]. Considerable assistance for breast cancer discernment and research funding has helped create advances in the diagnosis and treatment of breast cancer [14-16]. Surgery, Chemotherapy, Hormonal Therapy, Biological therapy, and Radiation therapy are the general medications practiced for cancer treatment, among which chemotherapy is mostly preferred by the medical fraternity.

To predict and to recommend the kind of treatment for cancer demands research at the molecular level and this involves cell lines, particularly, as in vitro models in cancer research. An MCF-7 cell line is a commonly used breast cancer cell line that has been promoted for more than 40 years by multiple research groups [17]. It proves to be a suitable model cell line for breast cancer investigations worldwide, including those regarding anticancer drugs [18]. It is Estrogen-positive (ER-positive) and progesterone receptor (PR)- positive [19]. MCF-7 is a poorly- hostile and non-protruding cell line [18], normally being considered to have low metastatic potential [19,20]. Despite certain advances in cancer therapy, still there is considerable demand for developing efficient therapeutic agents. In this study, the cytotoxicity of a synthetic chalcone derivative was investigated against MCF-7 cell line using MTT assay and for in silico study, the AutoDock 4.2.6 was adopted.

Chalcones are a class of natural open-chain flavonoids that are linked by a three-carbon spacer between two aromatic rings [21]. The α, β- unsaturated ketones and their analogs are well known for their uncountable biological activities and those are attributed to the carbonyl function with the double bond conjugate [22]. These compounds from flavonoids make them display antibacterial [23], anti-inflammatory [24], antifungal [25], anticancer [26], and many other pharmacological activities. The chalcone with α, β unsaturated carbonyl group, and chromanone moiety may increase the pharmaceutical efficiency since chromanone has good biological activity such as antioxidant, anti-leishmanial [27-28], antimicrobial [29]. The antivascular activity of

chalcones several tubulin-binding agents that inhibit tubulin assemblies, such as colchicine and vincristine, have recently been demonstrated to also disrupt tumor vasculature [29]. Presumably, these agents are capable of rapidly changing the shape of endothelial cells, thereby disrupting the endothelial cell layer surrounding blood vessels and exposing underlying basement membranes [30]. The change in the shape of endothelial cells leads to a loss of blood flow to the tumor, resulting in tumor necrosis [31]. This process is generally selective, and quiescent cells remain unaffected. Due to the unforeseen biological activity spectrum of chalcones and their analogs [32], we have focused on the synthesis and investigation of one such derivative and presenting the results in this communication. In the future, an attempt will be taken to conduct in vivo experiments to prove the efficaciousness of the title compound against cancer cell proliferation and to recommend its use in the field of drug designing.

The synthesis procedure and brief note on the characterization techniques and tools are given under Materials and methods. Detailed discussions on the derived results are arranged under results and discussion which is followed by the conclusion. The figures and tables are given at the appropriate places.

2. MATERIALS AND METHODS

2.1 Method of Preparation

All chemicals and solvents used in this study were purchased from Sigma Aldrich and Spectro chem. Pvt Ltd, Chennai, as high purity materials and used as such without any further purification. The title compound, $C_{18}H_{16}O_4$, was synthesized by base catalyst Claisen-Schmidt condensation reaction. During the synthesis process, an aqueous solution of NaOH (10%, 10 mL) was added to a mixture of 2,3-dihydro-4H-1-benzopyran-4-one and 2,4-dimethoxy benzaldehyde in 95% ethanol. The reaction mixture was stirred for 2 h and left overnight. A dark yellow colored product was obtained after filtering and is washed with ice-cold water. The product is then recrystallized in ethanol and yellow-colored transparent crystals of diffraction quality were obtained after seven days (m.p: 368 K; Yield-90%).

2.2 Chemical Characterization

The crystal data were collected using a diffraction quality crystal of size 0.200x0.200x 0.150mm on the goniometer head of the BRUKER AXS KAPPA APEX2-CCD diffractometer with MoKα (λ = 0.71073 Å) as an X-ray radiation source from Sophisticated Analytical Instruments Facility(SAIF), IITM, Chennai. The 3D crystal structure of the title molecule, $C_{18}H_{16}O_4$, was solved and refined using the SHEL-XS 97 [33] and SHEL-XL/XT-14 [34] software, respectively, by employing a full-matrix least-squares procedure on F^2. The Program PLATON [35] a Multipurpose Crystallographic tool was utilized to calculate the crystal parameters such as bond lengths, bond angles, torsion angles, dihedral angles, intra and intermolecular interactions, and conformation of the ring systems.

2.3 Hirshfeld Surfaces and Energy Frameworks Investigation

2.3.1 Hirshfeld surfaces

The Hirshfeld surfaces, two-dimensional fingerprint plots, and the colour-coded interaction energies mapping were generated to recognize and quantify the weak intermolecular interactions, using the software program Crystal
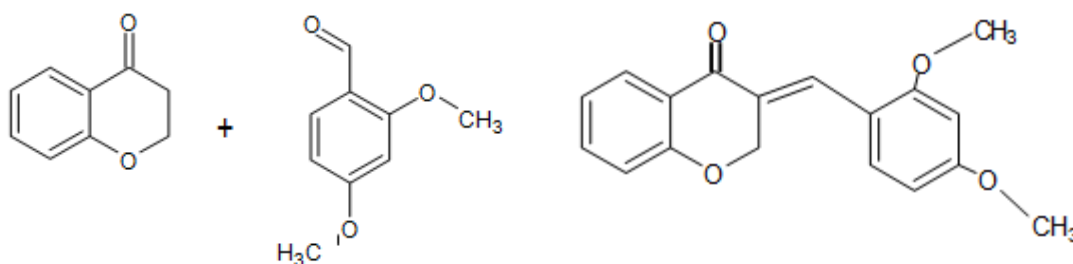

Fig. 1. Reaction scheme of DBDB

Fig. 2. DBDB Crystal

Explorer 17.5 [36]. In the recent past, the analysis of calculated Hirshfeld surfaces has become an indispensable tool for crystallographers and crystal designers, as this supplements information regarding the role of weak intermolecular interactions in the packing of molecules in crystals. These are surfaces wherein the ratio between the density weight function of the pro-molecule and the pro-crystal is 0.5a.u. (isosurface). Unlike van der Waals surface, these surfaces take into account the nearest neighbouring molecules, and thus provide details about intermolecular interactions [37, 38]. The surface properties to be mapped over this surface were d_i and d_e, the internal and external distances of an atom to the developed Hirshfeld surface. Compartmentalization of the generated surface using d_i and d_e values in a pair (d_i, d_e) and fitting into the intervals of 0.2 Å results in the generation of 2D fingerprint plots. In addition, these (d_i, d_e) pairs when normalized with respect to the van der Waals radii of their respective atoms results in the d_{norm} surface. The red color on the d_{norm} surface represents contacts shorter than the sum of the van der Waals radii of the two atoms resulting in a negative value. Contacts with lengths approximate to the van der Waals limit are colored white, and blue color illustrates longer contacts.

The Hirshfeld surfaces mapped over the molecular electrostatic potential can be generated using the computational software package Tonto [39], incorporated into the Crystal Explorer 17.5 program, which authorizes the visualization of the donors and acceptors of intermolecular interactions via blue and red regions around the participating atoms corresponding to positive and negative electrostatic potential on the surface, respectively. In addition, Hartree-Fock/DFT (HF/DFT) theory-based wave-function calculations and surface generation can be effected using Tonto, a popular quantum chemistry package that may replace other packages like Gaussian16 [40].

The shape-index is an approximate quantification of the geometrical shape (triangle), which is sensitive even to minute changes in surface shape (flat region), whereas Hirshfeld surface mapped on the surface property curvedness is the measure of the flatness of the regions particularly ring systems, with high curvedness is highlighted as dark-blue boundaries. These two surfaces analysis introduced by Koendrink [41, 42], provide additional information regarding the molecular packing within the crystal. The presences of adjacent blue and red triangles/flat regions inside the ring systems over shape-index/curvedness are illustrating the existence of π…π stacking interactions. Also, shape-index > 1 or < 1 represents the donor and acceptor atoms of intermolecular interaction, respectively.

Hirshfeld surface which comprises d_e and d_i in pair can be utilized to generate 2D fingerprint plots [43,44] representing the contribution due to various interatomic interactions. The colour of each segment on the surface relative to the area of a (d_e, d_i) pair is acknowledged as the supplement from different interatomic contacts. The frequency of occurrence of the interatomic (specific) interactions varies as blue-green-red, which illustrate the potential contribution to the total Hirshfeld surface changes as lowest-moderate-largest. The delineated 2D fingerprint plots obtained from the total 2D fingerprint plot can be an effective tool to derive the complex molecular interaction details hidden in a crystal.

2.4 Energy Frameworks

A new computational and graphical tool to calculate pairwise intermolecular interaction energies for organic and some inorganic molecular crystals were introduced by Turner *et al.*, 2014, whose employment in fabricating 'energy frameworks' provide an indomitable but new way to visualize the supramolecular architecture of molecular crystal structures [45], but with limitations i.e. energy frameworks were restricted to electrostatic and dispersion-energy

terms, in addition, total energies of the negative sign by assuming that these are the stabilizing energies the crystal structures of neutral molecules. Fundamentally, ionic crystals integrate large positive destabilizing (cation-cation and anion-anion), as well as a large negative (cation- anion) energies and these need to be represented as part of an energy-framework picture. To include these destabilizing energies, implementation of energy frameworks [45] now incorporates additional cylinders of different colors to energy-framework diagrams i.e. red for the electrostatic term, green dispersion, and blue total energy.

The pair-wise interaction energies within a crystal may be obtained by adding four energy components namely, electrostatic (E_{ele}), polarization (E_{pol}), dispersion (E_{dis}), and exchange-repulsion (E_{rep}) [26], and by fitting into the expression, viz $E_{tot} = E_{ele} + E_{pol} + E_{dis} + E_{rep}$, based on the energy model called counterpoise-corrected B3LYP-D2/6-31G (d,p). The calculation of interaction energies for crystal structures are generally simple, whereby users need to generate a cluster of molecules within a radius of 3.8 Å (i. e .the default value for molecules comprising light atoms) for a selected reference molecule and subsequently subject it to energy calculation upon setting the relevant parameters such as molecular charge, multiplicity, and energy model. The calculation of molecular interaction energies not only provide information about the four energy components but also supplement details about the existence of rotational symmetry operations, the centroid-to-centroid distance between the reference molecule and interacting molecules, and the number of pair(s) of interacting molecules with respect to the reference molecule. Visualization of these energies and their electrostatic and dispersion components, in the form of energy frameworks sheds light on the architecture of molecular crystals comprising metal coordination compounds, organic salts, solvates, and open-shell molecules.

2.5 Cytotoxicity and Anticancer Activity Investigation – MTT Assay

VERO cell line (normal) and MCF-7 cell lines (cancerous) were obtained from the National Centre for Cell Sciences, Pune (NCCS). The cells were maintained in Gibco Dulbecco's Modified Eagle Medium (DMEM) supplemented with 10% FBS, penicillin (100 U/mL), and streptomycin (100 µg/mL) in a humidified

atmosphere of 50 µg/mL CO_2 at 37°C. Cells (1×10^5/well) were plated in 24-well plates and incubated in 37°C with 5% CO_2 condition. After the cell reaches the confluence, the various concentrations of the sample were added and incubated for 24h. After incubation, the sample was removed from the well and washed with phosphate-buffered saline (pH 7.4) or DMEM without serum. 100µL/well (5mg/mL) of 0.5% 3-(4,5-dimethyl-2-thiazolyl)-2,5-diphenyl-tetrazolium bromide (MTT) was added and incubated for 4 h. After incubation, 1mL of DMSO was added to all the wells. The absorbance at 570nm was measured with a UV-Spectrophotometer using DMSO as the blank. Measurements were performed and the concentration required for a 50% inhibition (IC_{50}) was determined graphically. The anticancer activity test of the synthesized chalcone analogue on MCF-7 breast carcinoma was also performed by MTT assay [46].

2.6 In-Silico Analysis

The 3D crystal structure determination and the structure-activity relationship analysis play a predominant role in designing new drugs to fight against new diseases. AutoDock is an automated procedure for predicting the interaction of ligands with biomacromolecular targets, using the Lamarckian Genetic Algorithm along with the traditional genetic algorithms and simulated annealing. The empirical free energy scoring function, will provide reproducible docking results for ligands with approximately 10 flexible bonds, in addition to, visualizing conformations, visualizing interactions between ligands and proteins, and visualizing the affinity potentials created by AutoGrid. In the present work, the ligand (small molecule)- target (protein) interactions were studied using the AutoDock 4.2.6 software package [47], and the preparation of ligand and protein for the in-silico study and visualizing the interactions between them were done using PYMOL [48] a graphic software.

3. RESULTS AND DISCUSSION

3.1 Geometrical Parameters

The intensity data collection and refinement details are given in Table 1. In the title compound (Fig. 3), experimentally estimated C-C and C=C bond distances of the phenyl ring C1-C6 and C11-C16 are in the range 1.368(5)-1.403(4) and 1.364(4)-1.403(4)(Å), respectively, and the other C-C single bond distances in the structure are

lies between 1.450(4)-1.508(4) Å. The elongation observed in the C=C distances of the phenyl rings is attributed to the fusion between the rings about C5-C6 and the methoxy groups at C14 and C16. The C-O bond distances [1.364(4)-1.436(4)(Å)] and C=O distance of the chromenone ring is 1.220(4)Å (Table 3), and those are in good agreement with the similar reported structure [49-51]. The torsion angle C18-O4-C16-C11=175.97(1)°and C17-O3-C14-C15 = 0.16(1)°, indicates that the methoxy group is in +anti- periplanar (+ap) and syn-periplanar (+sp) orientation, respectively, with respect to the benzene ring (C11- C16). The carbonyl oxygen O2 tends to be coplanar with the chromenone ring, which is revealed by the symmetry between the bond angles C5-C7-O2 [121.7(3)] and C8-C7-O2 [122.5(3)°]. The dihedral angle between the mean aromatic planes is 57.42°, which shows the equatorial orientation with each other. In the title compound, the central cyclohexane ring [O1/C5-C9] adopts a distorted sofa conformation with ring puckering parameters; $q2=0.3690(2)$Å, $phi2=77.4(3)°$, $q3= -0.1627(2)$Å, $QT= 0.4033(2)$Å and $\theta= 113.79(2)°$ [52]. In the crystal packing, the adjacent molecules are linked via C-H…O hydrogen bonds [Table 2] forming a chain with deep bending and they are interlocked in such a way that there appears to generate 2D network (Fig. 4a), but not so because the chains running along 'a' axis are not linked by any intermolecular interaction. The packing of the molecules in the title compound viewed along 'a' axis is shown in Fig. 4a. The distorted sofa conformation taken up by the chromenone ring in Fig. 4b, and the unit cell packing for clarity drawn using mercury software is shown in Fig. 4c.
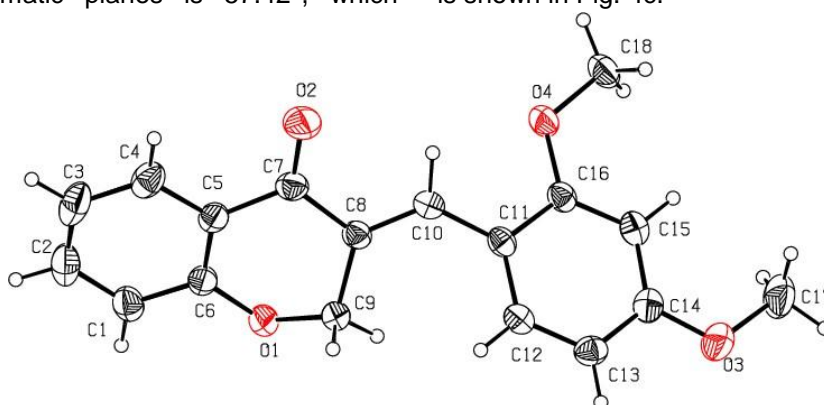
Fig. 3. Molecular structure of the title compound with atom labeling. Displacement ellipsoids are drawn at 30% probability level
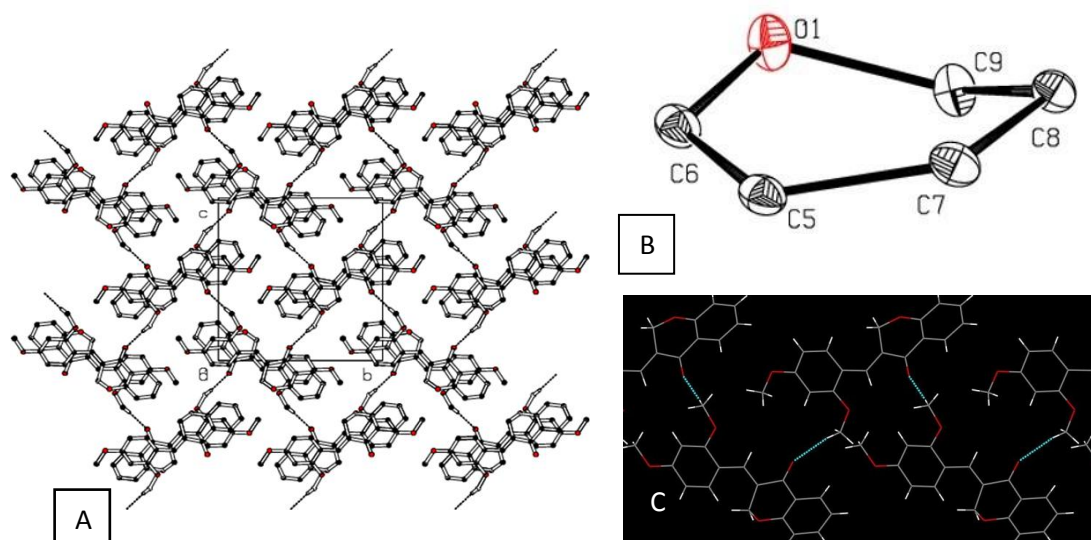
Fig. 4. (a) The crystal packing of the title compound, viewed along the 'a' axis with C-H…O hydrogen bonds (dashed line) (b) Ring conformation [Distorted Sofa] (c) Packing by mercury software

Table 1. Crystal data and structure refinement details

Crystal Data	DBDB
CCDC Number	1970618
Temperature (K)	296(2)
Wavelength(Å)	0.71073
Crystal system	Orthorhombic
Space group	$P2_1 2_1 2_1$
Unit cell dimensions(Å,°)	$\alpha=\beta=\gamma = 90$
	a =7.8756(5)
	b =13.4142(8)
	c =13.8440(8)
Volume(Å^3)	1462.55(15)
Z	4
Density (calculated)(Mg/m^3)	1.346
Absorption coefficient(mm^{-1})	0.095
F(000)	624
Crystal size(mm)	0.200 x 0.200 x 0.150
Theta range for data collection	2.943 to 26.415°.
Index ranges	-9≤h≤9, -16≤k≤16, -17≤l≤17
Reflections collected	35974
Independent reflections	2971 [R(int) = 0.0492]
Completeness to theta = 25.242°	99.5 %
Refinement method	Full-matrix least-squares on F^2
Data / restraints / parameters	2971 / 0 / 199
Goodness-of-fit on F^2	1.095
Final R indices [I>2sigma(I)]	R1 = 0.046, wR2 = 0.126
R indices (all data)	R1 = 0.057, wR2 = 0.142
Absolute structure parameter	-0.4(3)
Extinction coefficient	n/a
Largest diff. peak and hole(e.Å^{-3})	0.20 and -0.18

Table 2. Hydrogen bond geometry (Å,°)

D-H...A	d(D-H)	d(H...A)	d(D...A)	<(DHA)
C18-H18B ...O2 #1	0.96	2.44	3.368(5)	162

Symmetry code: #1 1-x,-1/2+y,1/2-z

Table 3. Selected Bond Length (Å), Bond Angle(°) and Torsion Angle(°)

Atoms	Bond distances (Å)	Atoms	Bond/torsion angles (°)	Atoms	torsion angles (°)
O1-C6	1.371(4)	C6-O1-C9	116.0(2)	C11-C10-C8-C9	-4.17
O1-C9	1.436(4)	C16-O4-C18	118.2(2)	C11-C10-C8-C7	175.5
O4-C16	1.366(4)	C6-C5-C4	118.6(3)	C16-C15-C14-O3	-179.41
O4-C18	1.428(4)	C6-C5-C7	120.5(3)	C16-C15-C14-C3	-0.39
O3-C14	1.364(4)	C4-C5-C7	120.7(3)	O2-C7-C8 -C9	171.66
O3-C17	1.434(5)	C8-C10-C11	129.4(3)	O2-C7-C8-C10	-8.04
O2-C7	1.220(4)	C12-C13-C14	119.5(3)	C5-C7-C8 -C9	-11.08
C9-C8	1.508(4)	C15-C16-C11	121.7(3)	C5-C7-C8-C10	169.23
C2-C3	1.3789(6)	C13-C12-C11	122.1(3)	O1-C6-C1-C2	-178.87
C4-C3	1.368(5)	C14-O3-C17	117.4(3)	C5-C6-C1-C2	-1.37

Atoms	Bond distances (Å)	Atoms	Bond/torsion angles (°)	Atoms	torsion angles (°)
C16-C15	1.387(4)	O1-C9-C8	113.6(2)	C6 -C1-C2-C3	-1.17
C16-C11	1.403(4)	O4-C16-C15	122.9(3)	C1-C2-C3-C4	2.35
C12-C13	1.374(5)	O4-C16-C11	115.4(2)	C5-C4-C3-C2	-0.98
C12-C11	1.393(4)	C6 -O1 -C9 -C8	-45.97	C4-C5-C7-O2	-8.39
C13-C14	1.386(4)	C9 -O1 -C6 -C5	24.03	C4-C5-C7-C8	174.32
C5-C6	1.386(4)	C9 -O1 -C6 -C1	-158.51	C7-C5-C6 -O1	6
C5-C4	1.403(4)	C18-O4 -C16-C15	-4.24	C7-C5-C6 -C1	-171.37
C5-C7	1.473(4)	C18-O4-C16-C11	175.97	C4-C5-C6-O1	-179.96
C10-C8	1.345(4)	C17-O3-C14-C13	-178.91	C4 -C5-C6-C1	2.67
C10-C11	1.450(4)	C17 -O3-C14 -C15	0.16	C7-C5-C4-C3	172.53
C15- C14	1.381(4)	O1-C9-C8-C10	-141.04	C6-C5-C4-C3	-1.49
C7-C8	1.476(4)	O1-C9-C8-C7	39.29	C8-C10 -C11-C16	150.56
C6-C1	1.392(4)	O4 -C16 -C15-C14	178.93	C8-C10-C11-C12	-35.41
C1-C2	1.369(5)	C11 -C16 -C15 -C14	-1.3	O4 -C16 -C11 - C12	-178.32
		O4 -C16 -C11 -C10	-3.91	C13 -C12-C11- C10	-175
		C15 -C16 -C11-C12	1.89	C12-C13 -C14 - O3	-179.49
		C15 -C16 -C11-C10	176.3	C12-C13 -C14- C15	1.41
		C11-C12-C13-H13	179.23	C6 -C5-C7-O2	165.52
		C11-C12-C13-C14	-0.77	C6 -C5-C7-C8	-11.77
		C13-C12-C11-C16	-0.84		

3.2 Hirshfeld Surfaces Analysis and Energy Frameworks Investigation

For the title molecule, the Hirshfeld surface mapped over d_{norm} was quantified with the default setting of arbitrary units range by using the validated Crystallographic Information File (CIF) as input to the Crystal Explorer 17.5. On rotation of the calculated plot Fig. 5(a), helps in identifying the bright-red spots near the methoxy hydrogen and carbonyl oxygen atoms indicate donors and acceptors of a potential C-H…O intermolecular interaction. The intensity of the red spots (bright, diminutive, and faint) can be utilized to specify the intermolecular interaction as potential hydrogen bonds, weak interactions, or short interatomic contacts. The Hirshfeld surfaces mapped over other surface properties namely shape-index and curvedness (Fig. 5b and d) can be effectively used to explain the role of weak intermolecular interactions such as C-H…π/π…π in stabilizing the crystal structure. Presence of adjacent blue and red regions (triangular shapes) within the ring systems on the Hirshfeld surface mapped over shape-index and the flat regions around the rings on the Hirshfeld surface mapped over curvedness are generally acknowledged as an indicator of C- H…π/π…π intermolecular contacts, but there are no such colored shapes either or flat regions over the generated Hirshfeld surface in the present study i.e the structure is devoid of C-H…π/π…π intermolecular contacts.

The calculated Hirshfeld surface of the title compound can also be analyzed in terms of two-dimensional fingerprint plots. As shown in Fig.6, the resultant two-dimensional fingerprint plot which includes all intermolecular contacts is the sum of the delineated plots due to various specific interactions (Fig. 6a-e). In general, the main contribution to the overall surface arises from H…H contacts, whereas the traditional hydrogen bonding always makes relatively small percentage contributions to the overall surface. In Fig. 6(b) and (d), the symmetrical forceps-like tips correspond to interactions H…C/C…H (15.2%) and H…O/O…H (13.9%) with di + de ≈ 3Å, which is slightly greater than the sum of the respective van der Waals radii, and indicative of the less likelihood for the C-H…π type of intermolecular contacts. The very weak π…π stacking interactions are evident from the fingerprint plot delineated into C…C (9%) contacts (Fig. 6c) as the rocket-like tip at de + di = 3.4Å.The fragment patches on the Hirshfeld surface provide convenient way to identify the nearest neighbour coordination environment of a molecule.

The simulated energy frameworks [37], were estimated to compare the topology of the intermolecular interactions in the title crystal. The pair-wise intermolecular interaction energies were calculated for a selected molecule in a cluster of molecules of radius 3.8 Å, using a counter poise-corrected DFT energy model CE-

B3LYP (Fig. 7a and Table.4) In the energy frameworks, the individual energy components such as E_{ele}, E_{dis} and E_{tot} are depicted as cylinders in red, green and blue colours, respectively, and with the radius of the corresponding cylinders proportional to the magnitude of interaction energy [44]. An analysis of the resultant energy frameworks is shown in Fig. 7b and reveals that the crystal packing of the title material is mainly stabilized by electrostatic and dispersive forces. These energies confirm that the interactions are predominantly dispersion based as is revealed by the energy-framework diagrams in Fig. 7b [53], where the magnitude of the dispersion energies almost mirrors the total energies; the electrostatic term though not influential, but largely cancelled by repulsion in each case.

3.3 In vitro Analysis Cytotoxicity

3.3.1 Cytotoxic effect on normal VERO cell line

The cytotoxic effect of the test compound on the normal VERO cell line was recorded by varying the sample concentration and quantifying the cell viability (Table 5), by following the standard MTT assay procedure [46]. A graph relating the sample concentration and the cell viability (Fig. 8) is extrapolated to calculate the IC_{50} (half maximal inhibitory concentration).
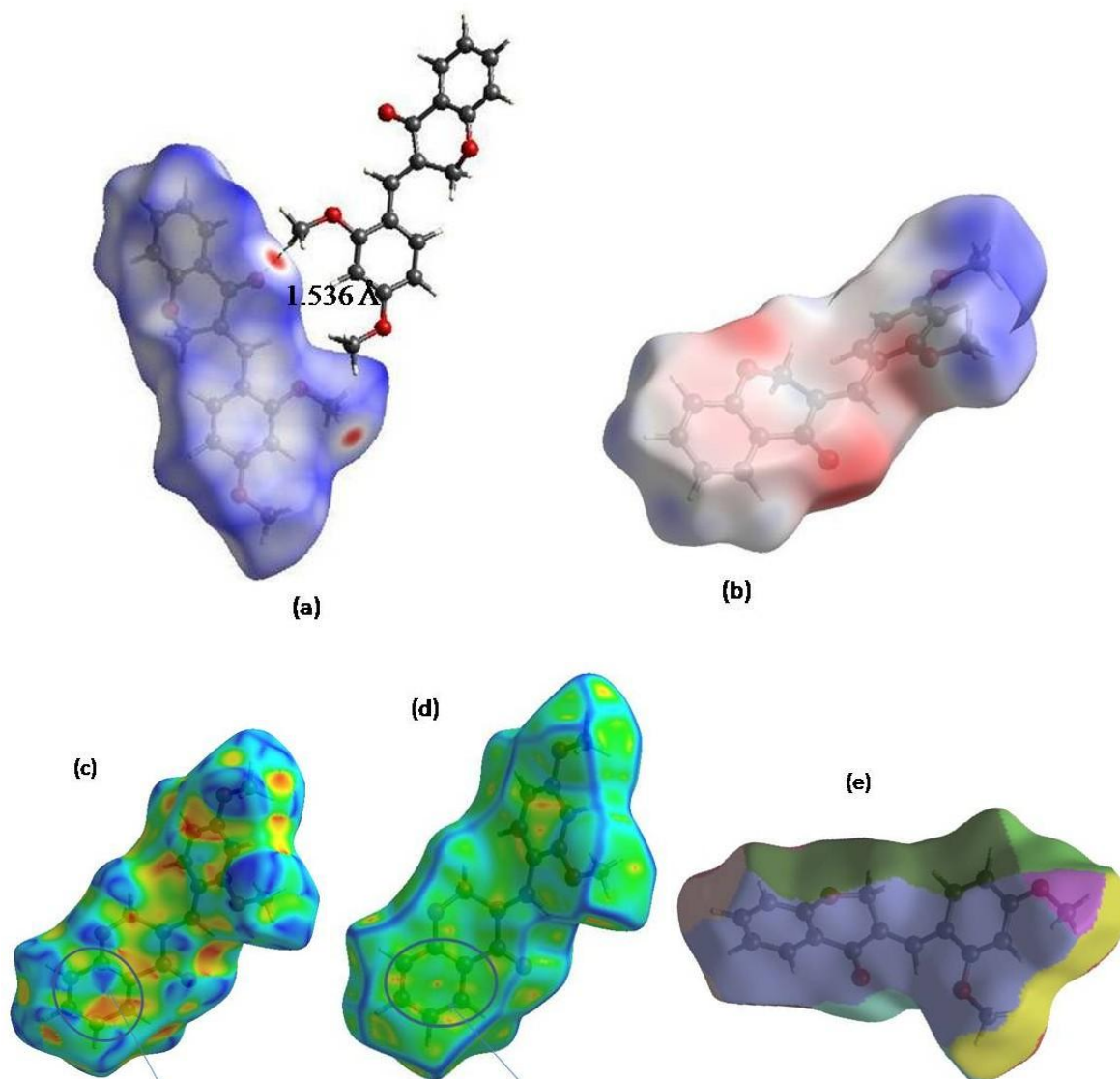

Fig. 5. Hirshfeld surface mapped over (a) d_{norm} (b) Electrostatic potential (c) Shape Index (d) Curvedness (e) Fragment patches

55

It is noticed that the concentration of the sample increases, the cell viability decreases slowly to 50% of its initial value at a half-maximal inhibitory concentration (IC_{50}) > 1000 µg/mL, and thus indicate less toxicity (Fig. 8, Table 6). Also, the morphological changes of Vero cells with respect to the varying sample concentration were compared to untreated cells, which show the decrease of normal cells as the sample concentration increases. The title compound exhibits 60.51% cell viability at a high concentration of 1000 µg/mL. Indicative of IC_{50} at concentration > 1000 µg/mL, and thus the compound is nontoxic on Vero cell line up to 1000 µg/mL (maximum testing concentration). The surface morphology changes recorded at a concentration of 1000 and 7.8µg/mL (available limit) are shown in Fig.9.
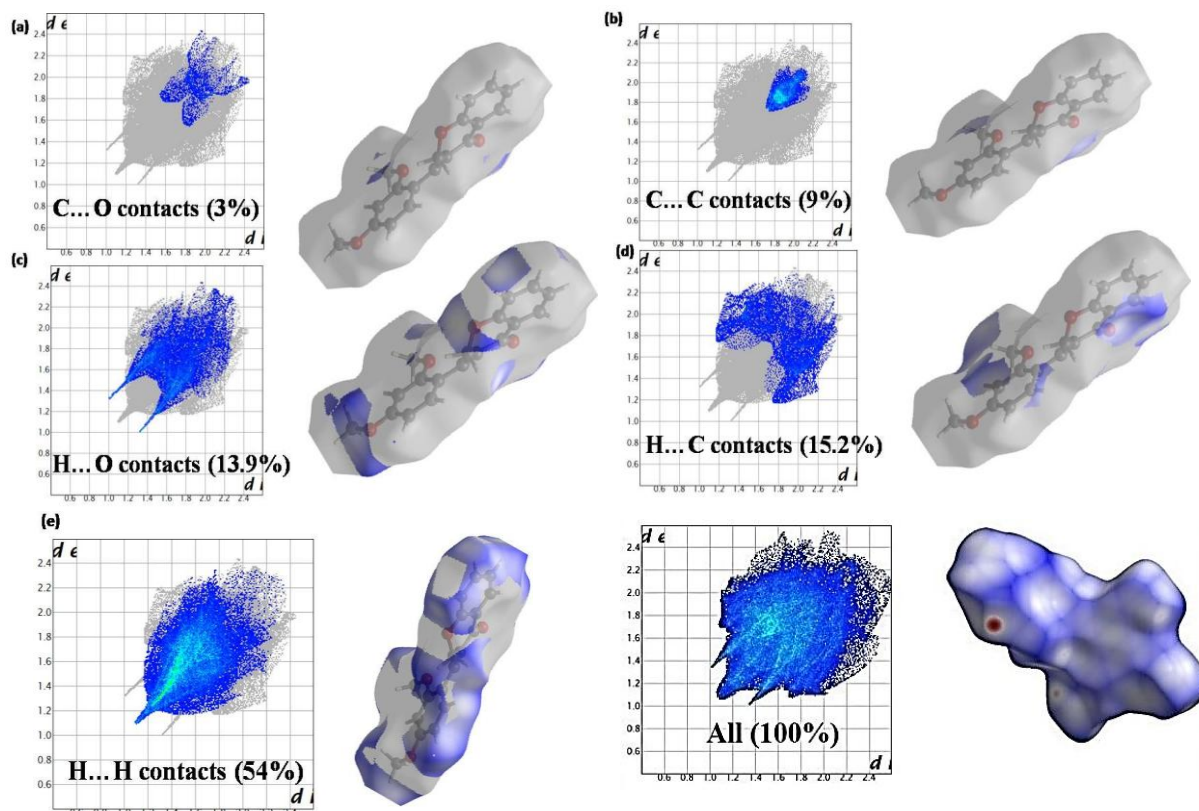
Fig. 6. Two-dimensional fingerprint plot for the title compound showing the delineated contributions: (a) C-O contacts, (b) C-C contacts, (c) H-O contacts, (d)H -C contacts, (e) H-H contacts and the whole

Table 4. Interaction energies (kJ mol $^{-1}$)

| Color	N	Sym.op	Electron density	R	Eelec	Epol	Edisp	Erep	Etotal
	2	x+1/2,- y+1/2, -z	B3LYP/631G(d,p)	4.00	-9.2	-4.7	-83.6	43.0	-59.3
	2	-x+1/2,-y,-z+1/2	B3LYP/631G(d,p)	9.44	-6.7	-2.2	-21.0	12.6	-19.2
	2	-x+1/2,-y,-z+1/2	B3LYP/631G(d,p)	10.38	-4.2	-2.6	-15.2	9.7	-13.6
	2	x,y,z	B3LYP/631G(d,p)	13.41	-5.8	-0.8	-9.5	4.9	-12.0
	2	-x+1/2,y+1/2,-z+1/2	B3LYP/631G(d,p)	9.79	-12.1	-4.5	-14.3	12.5	-20.8
	2	-x+1/2,y+1/2,-z+1/2	B3LYP/631G(d,p)	9.79	-2.1	-0.5	-16.7	9.0	-11.6
	2	-x,-y,-z	B3LYP/631G(d,p)	13.31	-0.4	-0.2	-4.0	0.5	-3.8
Energy Model				K_ele		K_pol		K_disp	K_rep
CE-B3LYP … B3LYP/6-31G(d,p) electron densities				1.057		0.740		0.871	0.618
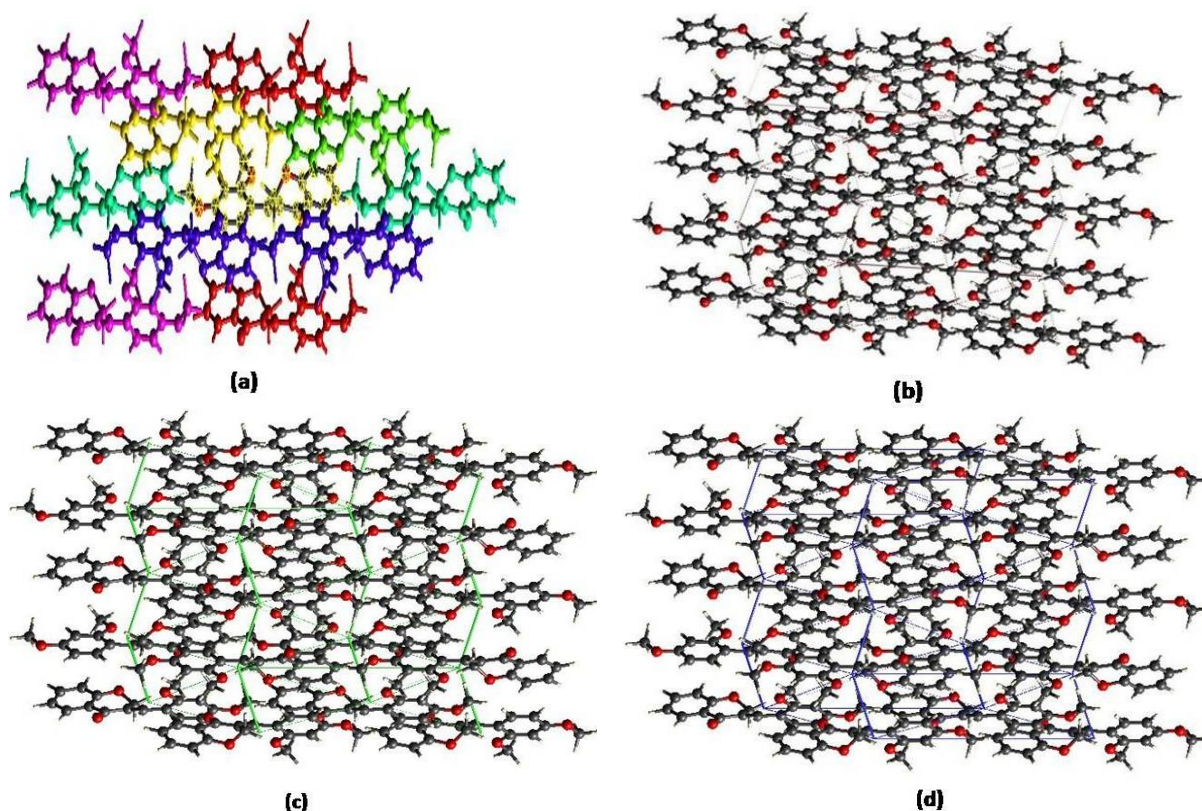
Fig. 7. (a) interaction between the selected molecule and the molecules around 3.8 å radius (b) electrostatic energy (c) dispersion energy and (d)total energy

Table 5. Cytotoxicity of the title compound

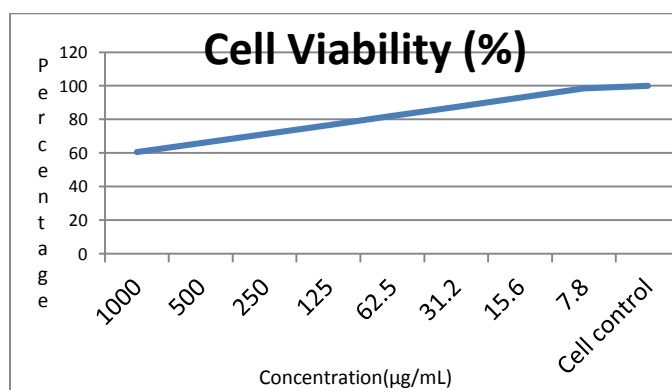| S. No	Concentration (µg/mL)	Dilutions	Absorbance (O.D)	Cell Viability (%)
1	1000	Neat	0.308	60.51
2	500	1:1	0.335	65.81
3	250	1:2	0.363	71.31
4	125	1:4	0.390	76.62
5	62.5	1:8	0.418	82.12
6	31.2	1:16	0.445	87.42
7	15.6	1:32	0.473	92.92
8	7.8	1:64	0.501	98.41
9	Cell control	-	0.509	100

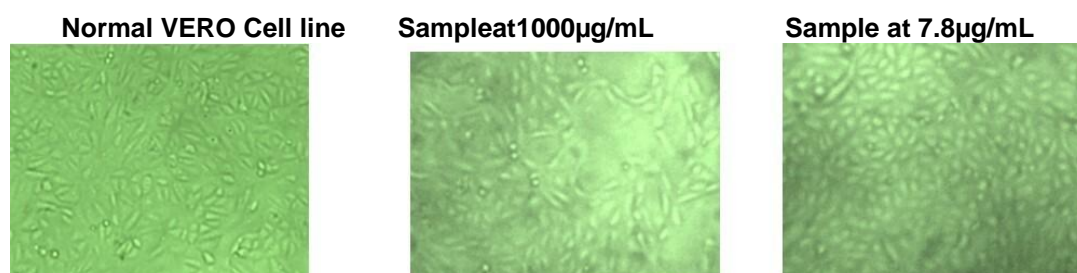**Fig. 8. Concentration vs Cell viability graph on extrapolation provide IC$_{50}$ value for the title Compound**

3.4 Anticancer Activity on MCF-7 Cell Lines

The anti-cancer proliferative activity of the synthesized compound on MCF-7 cell lines was evaluated by using an MTT assay method [46], in which the cell viability is measured for various sample concentrations (Table 6). It is observed that the cell viability decreases as the concentration of the sample increases and the concentration corresponding to $IC_{50}$ value of the compound is just around 7.8μg/mL (Fig.10), which demonstrate its efficacy as potential anticancer material in the field of drug designing. The recorded surface morphology changes of MCF-7 cells treated with the synthesized compound at 1000 and 7.8μg/mL concentrations are shown in Fig.11. The IC_{50} value corresponds to lower sample concentration of about 7.8μg/mL clearly illustrate the high toxicity against cancerous cells, and thus the title molecule can be considered as a lead drug candidate to fight against breast cancer

Table 6. Anticancer activity of title compounds on MCF-7 Cells

S.No	Concentration (μg/mL)	Dilutions	Absorbance (O.D)	Cell Viability (%)
1	1000	Neat	0.045	07.40
2	500	1:1	0.080	13.15
3	250	1:2	0.115	18.91
4	125	1:4	0.151	24.83
5	62.5	1:8	0.186	30.59
6	31.2	1:16	0.221	36.34
7	15.6	1:32	0.256	42.10
8	7.8	1:64	0.294	48.35
9	Cell control	-	0.608	100

Normal VERO Cell line   **Sampleat1000μg/mL**   **Sample at 7.8μg/mL**

Fig. 9. Morphological changes (Cytotoxic effect) of the title compound on normal Vero cell line at sample concentration of 1000 and 7.8μg/mL
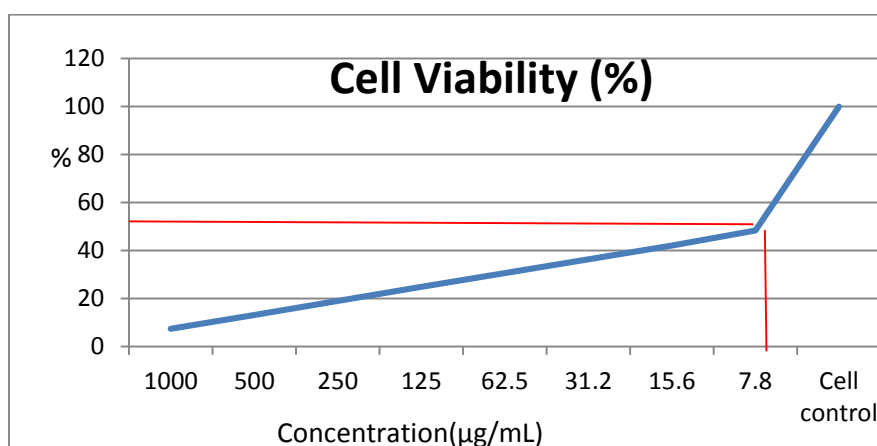
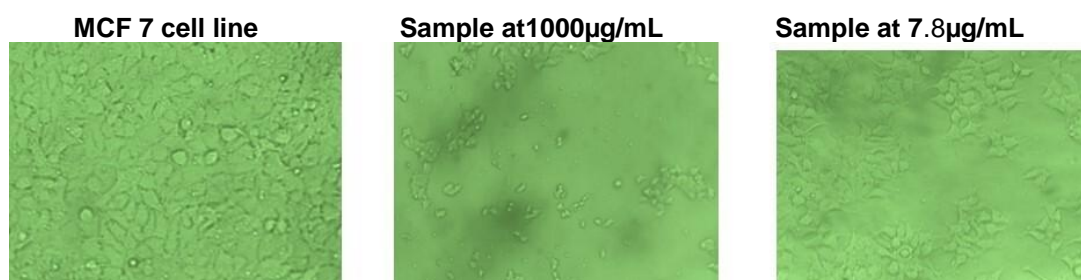**Fig. 10. Concentration vs. Cell viability plot showing the IC_{50} value for the title compound**

MCF 7 cell line	Sample at1000µg/mL	Sample at 7.8µg/mL

Fig. 11. Surface morphology Changes on MCF-7 Cell lines for the title Compound
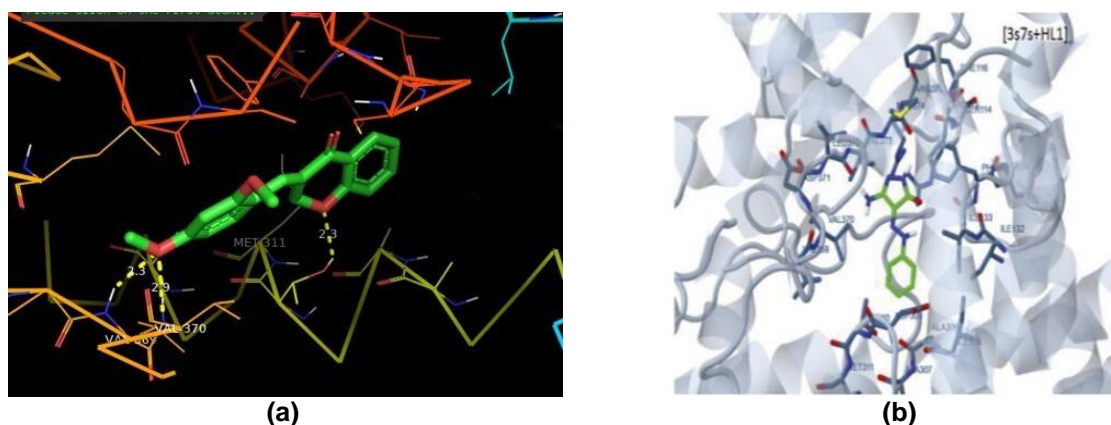

| **(a)** | **(b)** |

Fig. 12. PYMOL plot representing the active site interactions (a) between the ligand (DBDB) and the protein (3s7s) (b) between the co-crystal (triazole) and the protein (3s7s) protein (3s7s) and (b) Between the co-crystal and the protein (3s7s)

Table 7. Scoring functions obtained via molecular docking simulation

Run No.	Binding energy kcal/mol	Inhibition constant(Ki) µM	Intermolecular energy kcal/mol
1	-6.40	0.20	-7.29
2	**-9.90**	**0.55**	**-10.79**
3	-8.01	1.35	-10.02
4	-9.13	2.03	-9.68
5	-8.70	4.22	-9.59
6	-7.59	2.72	-8.49
7	-8.90	2.99	-9.79
8	-7.10	6.28	-7.99
9	-9.17	1.88	-10.07
10	-9.11	2.09	-10.01

Table 8. Binding site interactions and binding energies

Ligand	Run No./Pose	Binding site interaction	D-H…A (Å)	Binding energy kcal/mol
Co-crystal (triazole)	5	[VAL'370A)]N-H...O	3.3	8.70
		N-H…O[CYS'310(A)]	3.9	
Title molecule (DBDB)	2	N-H…O1[VAL'370(A)]	2.6	-9.90
		O…SG1[CYS'437(A)]	2.9	

59

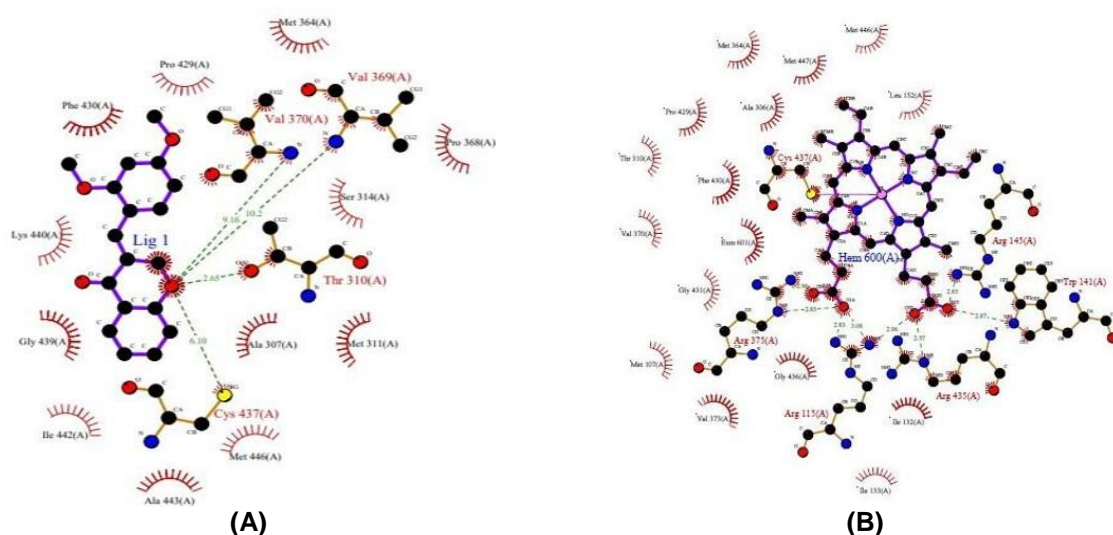**(A)**   **(B)**

Fig. 13. Lig plot representing the active site interactions (a) Between the ligand (DBDB) and the

3.4 Molecular Docking Investigation

Molecular docking analysis has been performed to identify the best pose in which the ligand (small molecule) perfectly fit into the active site of the target (protein) using AutoDock 4.2.6 software and PYMOL graphic software to visualize the molecular interactions. In this work, the 3D crystal structure of the reference drug complexed with the co-crystal triazole (PDB ID: 3s7s) [54] was downloaded from RCSB Protein Data Bank [55,56]. After preparing the ligand and protein for molecular docking, the co-crystal inhibitor was replaced by the title compound and the docking processes has initiated with the protein active site of grid spacing 0.375Å [57]. The docking process was continued for ten runs using AutoDock Tools 1.5.6, and the scoring functions including binding energy, inhibition constant, and intermolecular interaction energy was tabulated [Table7]. The protein active site interactions (hydrogen bonding interactions) along with binding energies were given in Table 8. The best fit interaction is defined by the lowest binding energy (-9.9kcal/mol) and the corresponding inhibition constant Ki (0.55µM) [Table 7]. In the present work, corresponding to run 2, the ligand interaction with 3s7s protein exhibits the lowest binding energy value of -9.90kcal/mol, which is illustrative of the excellent binding affinity between the ligand and the protein receptor. Also, the title molecule well fits into the binding site of protein with amino acid residues VAL'370(A) and CYS'437(A), and are in good agreement with the reported co-crystal complexed structure Fig 12 and 13 [58].

4. CONCLUSION

(3*E*)-3-(2, 4-Dimethoxy Benzyldene)-2,3-Dihydro-4H- Chromen-4-One (DBDB), a new chalcone derivative was synthesized using Claisen-Schmidt condensation reaction at room temperature. The grown crystal was studied for its 3D structure via the XRD technique and the calculated crystallographic parameters were found to be normal. Hirshfeld surfaces mapped over the surface properties such as d_{norm}, electrostatic potential, shape-index, and curvedness provide valuable information regarding the potential hydrogen bonding contacts, the positive and negative electrostatic potential regions, and the C-H…π and π...π stacking interactions. The calculation of pairwise intermolecular interaction energies described by the energy frameworks for the title molecule indicates the predominant contribution due to the dispersion energy. The 2D fingerprint plots of the total and the delineated Hirshfeld surfaces clearly explain the contribution resulting from various intermolecular contacts. In vitro analysis on normal (VERO) and cancerous (MCF 7) cell lines were performed to understand the cytotoxic effect of the title compound. It is observed that the present material is less toxic (with large cell viability) to normal cells but highly toxic (least cell viability) to cancerous cells. The combination of in vitro and in silico (molecular docking) method is followed to test and quantify the efficacy of the title material to be a potential drug candidate to treat breast cancer, and from the derived results we recommend that the synthesized material can be a lead material for pharmaceutical applications.

DISCLAIMER

The products used for this research are commonly and predominantly use products in our area of research and country. There is absolutely no conflict of interest between the authors and producers of the products because we do not intend to use these products as an avenue for any litigation but for the advancement of knowledge. Also, the research was not funded by the producing company rather it was funded by personal efforts of the authors.

COMPETING INTERESTS

Authors have declared that no competing interests exist.

REFERENCES

1. Available:http://www.pfizer.com/produ cts/cancer_in_asia.pdf (accessed01.05.15)
2. Available:http://www.cancer.org/acs/group s/content/@epidermiologysurveillance/web content/041787.pdf (acce ssed 01.05.15)
3. Available:https://www.cancer.gov (accessed 17.06.2021)
4. Buqué A, Bloy N, Perez-Lanzón M, Iribarren K, Humeau J, Pol JG, Galluzzi L. Immunoprophylactic and immunotherapeutic control of hormone receptor-positive breast cancer. Nature Communications. 2020;11(1). DOI:10.1038/s41467-020-17644-0
5. Hogan KA, Chini CCS, Chini EN. The multi-faceted ecto-enzyme CD38: roles in immunomodulation, cancer, aging, and metabolic diseases. Front Immunol. 2019;10:1187. DOI:https://doi.org/10.3389/fimmu.2019.01 1871 11 1
6. LUNGevity Foundation. Types of Lung Cancer. Available:https://lungevity.org/for-patients-caregivers/lung-cancer-101/types-of-lungcancer Accessed May 2021
7. American Society of Clinical Oncology (ASCO). Lung Cancer – Non-Small Cell: Introduction. Available:http://www.cancer.net/cancertype s/lung-cancer-non-small-cell/introduction Accessed May 2021
8. Manson JE, et al. Vitamin D supplements and prevention of cancer and cardiovascular disease. N. Engl. J. Med. 2019;380:33–44. DOI: 10.1056/NEJMoa1809944
9. Galluzzi L. et al. Consensus guidelines for the definition, detection and interpretation of immunogenic cell death. J. Immunother. Cancer. 2020;8:e000337. DOI: 10.1136/jitc-2019-000337
10. Go2 Foundation for Lung Cancer. Types of Lung Cancer. Available:https://go2foundation.org/what-is-lung-cancer/types-of-lungcancer/ Accessed May 2021
11. Bray F, Ferlay J, Soerjomataram I, Siegel RL, Torre LA, Jemal A. Global cancer statistics 2018: GLOBOCAN estimates of incidence and mortality worldwide for 36 cancers in 185 countries. CA: A Cancer Journal for Clinicians. 2018 Nov;68(6):394-424. DOI:https://doi.org/10.3322/caac.21492
12. World Cancer Report 2014. World Health Organization. 2014;Chapter 5.2. ISBN 978-92-830429-9.
13. Yue Y, Ye K, Lu J, Wang X, Zhang S, Liu L, Yang B, Nassar K, Xu X, Pang X, et al. Probiotic strain Lactobacillus plantarum YYC-3 prevents colon cancer in mice by regulating the tumour microenvironment. Biomed Pharm. 2020;127:110-159. DOI:https://doi.org/10.1016/j.biopha.2020.1 10159
14. Spencer CN, Gopalakrishnan V, McQuade J, Andrews MC, Helmink B, Khan MW, Sirmans E, Haydu L, Cogdill A, Burton E, et al. The Gut Microbiome (GM) and Immunotherapy Response Are Influenced by Host Lifestyle Factors. Tumor. Biol.; 2019. DOI:https://doi.org/10.3390/nu12082226
15. Ippolito L, Morandi A, Taddei ML, Parri M, Comito G, Iscaro A, Raspollini MR, Magherini F, Rapizzi E, Masquelier J, et al. Cancer-associated fibroblasts promote prostate cancer malignancy via metabolic rewiring and mitochondrial transfer. Oncogene. 2019;38:5339–5355. DOI:https://doi.org/10.1038/s41388-019-0805-7
16. Patel SP, Othus M, Chae YK, Giles FJ, Hansel DE, Singh PP, Fontaine A, Shah MH, Kasi A, Al Baghdadi T, et al. A Phase II Basket Trial of Dual Anti-CTLA-4 and Anti-PD-1 Blockade in Rare Tumors (DART SWOG 1609) in Patients with Nonpancreatic Neuroendocrine Tumors. Clin. Cancer Res. 2020;26:2290–2296. DOI: 10.1158/1078-0432.CCR-19-3356
17. Gunduz M, GunduzE,Baguley BC, Leung E. Heterogeneity of phenotype in breast

cancer cell lines. in: breast cancer – carcinogenesis. Cell Growth and Signalling Pathways (Gunduz M, Gunduz E (eds.). Rijeka, InTech. 2011;245-256.

18. Gunduz M, Gunduz E, Shirazi FH. Remarks in successful cellular investigations for fighting breast cancer using novel synthetic compounds. In: Breast Cancer – Focusing Tumor Microenvironment, Stem Cells and Metastasis (Gunduz M, Gunduz E (eds.). Rijeka, InTech. 2011;85-102.
DOI:https://doi.org/10.1055/s-2006-957853

19. Gest C, Joimel U, Huang L, Pritchard LL, Petit A, Dulong C, Buquet C, Hu CQ, Mirshahi P, Laurent M, Fauvel-Lafève F. Rac3 induces a molecular pathway triggering breast cancer cell aggressiveness: differences in MDA-MB-231 and MCF-7 breast cancer cell lines. BMC cancer. 2013 Dec;13(1):1-4.
DOI:https://doi.org/10.1186/1471-2407-13-63

20. Bassiouni W, Daabees T, Norel X, Senbel AM Hypoactivity of rat detrusor muscle in a model of cystitis: exacerbation by non-selective COX inhibitors and amelioration by a selective DP1 receptor antagonist. Naunyn-Schmiedeberg's Arch Pharmacol. 2019;392:437–450.

21. Ducki S, Hadfield JA, Lawrence NJ, Liu CY, McGown AT, Zhang X. Isolation of E-1-(4′-Hydroxyphenyl)-but-1-en-2-one from Scutellariabarbata. Planta Medica. 1996 Apr;62(02):185-186.
DOI:https://doi.org/10.1055/s-2006-957853

22. Singh P, Anand A, Kumar V. Recent developments in biological activities of chalcones: A mini review. European Journal of Medicinal Chemistry. 2014;85:758-777.
DOI:https://doi.org/10.1016/j.ejmech.2014.08.033

23. Ansari FL, Nazir S, Noureen H, Mirza B. Combinatorial synthesis and antibacterial evaluation of an indexed chalcone library. Chemistry & Biodiversity. 2005;2(12):1656-1664.
DOI:https://doi.org/10.1002/cbdv.200590135

24. Hsieh HK, Tsao LT, Wang JP, Lin CN. Synthesis and anti-inflammatory effect of chalcones. Journal of Pharmacy and Pharmacology. 2000;52(2):163-171.
DOI:https://doi.org/10.1211/0022357001773814

25. Lahtchev KL, Batovska DI, St PP, Ubiyvovk VM, Sibirny AA. Antifungal activity of chalcones: A mechanistic study using various yeast strains. European Journal of Medicinal Chemistry. 2008;43 (10):2220-2228.
DOI:https://doi.org/10.1016/j.ejmech.2007.12.027

26. Mahapatra DK, Bharti SK, Asati V. Anticancer chalcones: Structural and molecular target perspectives. European Journal of Medicinal Chemistry. 2015;98:69-114.
DOII:https://doi.org/10.1016/j.ejmech.2015.05.004

27. Sharma UK, Sharma AK, Gupta A, Kumar R, Pandey AK, Pandey AK. Pharmacological activities of cinnamaldehyde and eugenol: Antioxidant, cytotoxic and anti-leishmanial aspects. Cell Mol Biol (Noisy le Grand). 2017;63(6).

28. Naz R, Roberts TH, Bano A, Nosheen A, Yasmin H, Hassan MN, Anwar Z. GC-MS analysis, antimicrobial, antioxidant, antilipoxygenase and cytotoxic activities of Jacaranda mimosifolia methanol leaf extracts and fractions. PLOS ONE. 2020;15(7):e0236319.
DOI:10.1371/journal.pone.0236319

29. Montazerozohori M, Mohammadi H, Masoudiasl A, Nasr-Esfahani M, Naghiha R, Assoud A. Crystal structure, DFT study, antimicrobial properties and DNA cleavage potential and thermal behavior of some new mercury complexes. Journal of the Iranian Chemical Society. 2017;14(2): 297-312.
DOI:https://doi.org/10.1007/s13738-016-0978-8

30. Edwards ML, Stemerick DM, Sunkara PS. Chalcones: a new class of antimitotic agents. Journal of medicinal chemistry. 1990 Jul;33(7):1948-1954.
DOI:https://doi.org/10.1021/jm00169a021

31. Ducki S. The development of chalcones as promising anticancer agents. IDrugs. 2007 Jan 1;10(1):42.

32. De Vincenzo R, Ferlini C, Distefano M, Gaggini C, Riva A, Bombardelli E, Morazzoni P, Valenti P, Belluti F, Ranelletti FO, Mancuso S. In vitro evaluation of newly developed chalcone analogues in human cancer cells. Cancer chemotherapy and pharmacology. 2000; 46(4): 305-312.

33. Sheldrick GM, SHELXS97 S. University of Göttingen.

34. (a) G.M. Sheldrick, Crystal structure refinement with SHELXL. Acta Crystallographica Section C: Structural Chemistry. C(71) (2015) 3-8.
DOI:https://doi.org/10.1107/S20532296140 24218
(b)G.M. Sheldrick, SHELXT–Integrated space-group and crystal-structure determination. Acta Crystallographica Section A: Foundations and Advances. A(71)(2015) 3-8.
DOI:https://doi.org/10.1107/S20532733140 26370

35. Spek AL. Acta Cryst. 2009;D65:148–155.

36. Turner MJ, MacKinnon JJ, Wolff SK, Grimwood DJ, Spackman PR, Jayatilaka D, Spackma MA. Crystal ExplorerVer. 17.5. University of Western Avustralia, Pert. 2017;2:133-144.

37. McKinnon JJ, Jayatilaka D, Spackman MA. Towards quantitative analysis ofintermolecular rinteractions with Hirshfeld surfaces. Chemical Communications. 2007;(37):3814-3906.
DOI:https://doi.org/10.1039/B704980C

38. Spackman MA, Jayatilaka D. Hirshfeld surface analysis. Cryst Eng Comm. 2009;11(1):19-32.
DOI: 10.1039/B818330A

39. Jayatilaka D, Grimwood DJ. Tonto: A fortran based object-oriented system for quantum chemistry and crystallography. In International Conference on Computational Science. Springer, Berlin, Heidelber. 2003 Jun 2;142-151.

40. Frisch MJ, Trucks GW, Schlegel HB, Scuseria GE, Robb MA, Cheeseman JR, Scalmani G, Barone V, Petersson GA, Nakatsuji H, Li X. Gaussian 16 revision a. 03. 2016; gaussian inc. Wallingford CT. 2016;2(4).

41. Koenderink JJ. Solid Shape. Cambridge MA: MIT Press; 1990.

42. Koenderink JJ, van Doorn, A. J.Image Vis. Comput. 1992;10,557–564.

43. Spackman MA, McKinnon JJ. Fingerprinting intermolecular interactions in molecular crystals. Cryst Eng Comm. 2002 Jul 18;4(66):378-392.
DOI: 10.1039/b203191b

44. McKinnon JJ, Spackman MA, Mitchell AS. Novel tools for visualizing and exploring intermolecular interactions in molecular crystals. Acta Crystallographica Section B: Structural Science. 2004 Dec 1;60(6):627-68.

45. Turner MJ, Grabowsky S, Jayatilaka D, Spackman MA. Accurate and efficient model energies for exploring intermolecular interactions in molecular crystals. The Journal of Physical Chemistry Letters. 2014 Dec 18;5(24):4249-4255.
DOI:https://doi.org/10.1021/jz502271c

46. Mosmann T. Rapid colorimetric assay for cellular growth and survival: application to proliferation and cytotoxicity assays. J. Immunol. Methods. 1983;65: 55-63.

47. Morris GM. Goodsell DS, Halliday RS, Huey R,Hart WE, Belew RK, Olson AJ. Automated docking using a Lamarckian genetic algorithm and empiricalbinding free energy function, J. Comput. Chem. 1998; 19:1639-1662.

48. The PyMOL Molecular Graphics System, LLC, Schrodinger. 2009;Version 15.0.4.

49. Biruntha K, Reuben Jonathan D, Mohamooda Sumaya U, Dravida Thendral ER, Usha G. (3E)-3- [(2E)-3-(4-Methoxyphenyl) prop-2-enylidene]-2, 3-dihydro-4H-chromen-4-one. IUCrData. 2018 Jun 28;3(6):x180829.
DOI:https://doi.org/10.1107/S24143146180 08295

50. HaroonM, Akhtar T, Tahir MN. Crystal structure of (E)-2-(4-chlorobenzylidene)-3, 4- dihydronaphthalen-1 (2H)-one: a second monoclinic polymorph. Acta Crystallographica Section E: Crystallographic Communications. 2015 Oct 1;71(10):o741-742..
DOI:https://doi.org/10.1107/S20569890150 16151

51. Gopaul K, Shaikh MM, Koorbanally NA, Ramjugernath D, Omondi B. (E)3-(4-Cyclohexyl-3-fluorobenzylidene)chroman-4-one. ActaCryst. 2012;68:o1972

52. Cremer DT, Pople JA. General definition of ring puckering coordinates. Journal of the American Chemical Society. 1975 Mar;97(6):1354-1358.
DOI:https://doi.org/10.1021/ja00839a011

53. Maloney AG, Wood PA, Parsons S. Intermolecular interaction energies in transition metal coordination compounds. CrystEngComm. 2015;17(48):9300-9310.
DOI:10.1039/C5CE01522G

54. Abdellattif MH, Hussien MA, Alzahrani E, IJPSR 2018;9:1000.

55. Althagafi I, El-Metwaly N, Farghaly TA, Molecules. 2019;24:1741.

DOI:https://doi.org/10.3390/molecules2409
1741

56. Fleming I. Frontier orbital's and organic chemical reactions. Wiley, London; 1976.

57. Morales-Ríos MS, López-Camacho PY, Suárez-Castillo OR, Joseph-Nathan P. Trapping enols of esters and lactones with diazomethane. Tetrahedron Letters. 2007 Mar 26;48(13):2245-2249.

DOI:https://doi.org/10.1016/j.tetlet.2007.02.006

58. Nielsen SF, Christensen SB, Cruciani G, Kharazmi A, Liljefors T. Antileishmanial chalcones: Statistical design, synthesis, and three-dimensional quantitative structure− activity relationship analysis. Journal of Medicinal Chemistry. 1998 Nov 19;41(24):4819-4832.

DOI:https://doi.org/10.1021/jm980410m